Downloaded from orbit.dtu.dk on: May 06, 2023

DTU Library

Nonlinear Eddy Viscosity Models applied to Wind Turbine Wakes

Laan, van der, Paul Maarten; Sørensen, Niels N.; Réthoré, Pierre-Elouan; Mann, Jakob; Kelly, Mark C.; Schepers, J.G.

Published in:
Proceedings of the 2013 International Conference on aerodynamics of Offshore Wind Energy Systems and wakes (ICOWES2013)

Publication date:
2013

Document Version
Publisher's PDF, also known as Version of record

Link back to DTU Orbit

Citation (APA):
Laan, van der, P. M., Sørensen, N. N., Réthoré, P-E., Mann, J., Kelly, M. C., & Schepers, J. G. (2013). Nonlinear Eddy Viscosity Models applied to Wind Turbine Wakes. In *Proceedings of the 2013 International Conference on aerodynamics of Offshore Wind Energy Systems and wakes (ICOWES2013)* (pp. 514-525). Technical University of Denmark.

General rights
Copyright and moral rights for the publications made accessible in the public portal are retained by the authors and/or other copyright owners and it is a condition of accessing publications that users recognise and abide by the legal requirements associated with these rights.

- Users may download and print one copy of any publication from the public portal for the purpose of private study or research.
- You may not further distribute the material or use it for any profit-making activity or commercial gain
- You may freely distribute the URL identifying the publication in the public portal

If you believe that this document breaches copyright please contact us providing details, and we will remove access to the work immediately and investigate your claim.

Nonlinear Eddy Viscosity Models applied to Wind Turbine Wakes

M.P. van der Laan[1], N. N. Sørensen[1], P.-E. Réthoré[1], J. Mann[1], M.C. Kelly[1], J.G. Schepers[2]

[1]Technical University of Denmark, DTU Wind Energy, Risø Campus, Building 114, Frederiksborgvej 399, 4000 Roskilde, Denmark, plaa@dtu.dk
[2]Energy Research Centre of the Netherlands (ECN), Wind Energy, Petten, 1755ZG, The Netherlands

27 March 2013

ABSTRACT

The linear $k-\varepsilon$ eddy viscosity model and modified versions of two existing nonlinear eddy viscosity models are applied to single wind turbine wake simulations using a Reynolds Averaged Navier-Stokes code. Results are compared with field wake measurements. The nonlinear models give better results compared to the linear model, however, high turbulence levels can produce numerical instabilities.

1 INTRODUCTION

The energy losses in a wind farm due to interaction of wakes can often range between 10% to 20% [1]. Therefore, reliable and practical modeling of the influence of wind turbine wakes in wind farms is necessary in order to estimate the wind farm annual energy production. Computational Fluid Dynamics (CFD) methods as Large Eddy Simulation (LES) or Reynolds Average Navier-Stokes (RANS) can be employed to simulate wake effects. Results of LES has proven to compare well with results of wake measurements [2] but the computational costs are still high. RANS is roughly two orders of computational effort cheaper than LES, however, previous studies have shown that the most widely used turbulence models in RANS, e.g. the linear $k-\varepsilon$ eddy viscosity model (EVM), fail to predict the wake deficit and the Reynolds-stresses in a wake [3]. The basis of a linear EVM is the eddy viscosity hypothesis of Boussinesq that linearly relates the Reynolds-stresses to the symmetrical part of the velocity gradients (i.e. the strain rate tensor $S_{ij} = 1/2\,(U_{i,j} + U_{j,i})$) [4]. As a result, the linear EVM cannot represent effects caused by the anti symmetric part of the velocity gradients (i.e. the vorticity tensor $\Omega_{ij} = 1/2\,(U_{i,j} - U_{j,i})$) and effects caused by products of the velocity gradients, e.g.: normal Reynolds-stress anisotropy, swirl and stream line curvature. A turbulence model that can include all these effects is the nonlinear eddy viscosity model (NLEVM) of Apsley and Leschziner [5], which is based on an extended eddy viscosity hypothesis where nonlinear terms of products of S_{ij} and Ω_{ij} are present up to the third order. The cubic NLEVM is used in this research with minor modifications such that the user can control the (undisturbed) turbulence intensity. In addition to the cubic NLEVM of Apsley and Leschziner, the quartic NLEVM of Taulbee [6] is investigated, which was previously studied by Crespo et al. [7]. The background, definition and modifications of the cubic NLEVM and the quartic NLEVM are given in Sec. 2. In Sec. 3 both NLEVMs are tested and compared with field measurements of two single wind turbine wake cases.

In this paper tensors are written with bold symbols and index notation: $\mathbf{a} \equiv a_{ij}$. Traces of tensors are written as: $\{\mathbf{a}\} \equiv a_{ii}$. Summation is only done with roman indices. Greek indices are not summed up. In addition, a tensor product is written as: $\mathbf{as} \equiv a_{ik}s_{kj}$ and $\{\mathbf{as}\} \equiv a_{kl}s_{lk}$.

2 NONLINEAR EDDY VISCOSITY MODELS

The background and definition of the cubic and the quartic NLEVM are discussed in Sec. 2.1. The calibration of the model constants is addressed in Sec. 2.2 and Sec. 2.3. Limiter functions for guaranteeing positive, bounded eddy viscosity are presented in Sec. 2.4 and Sec. 2.5, respectively. Sec. 2.6 provides details about the implementation.

2.1 Background and definition

The foundations of the nonlinear stress-strain relationship used in the NLEVMs is based on algebraic Reynolds-stress models (ARSMs) where the Reynolds-stress is calculated via an implicit algebraic set of equations. The ARSMs are derived from differential Reynolds-stress models by using Rodi's weak assumption [8]. In addition, the pressure-strain model of Launder et al. [9] is used to obtain the full algebraic set of equations:

$$\mathbf{a} \quad = \quad -\alpha\mathbf{s} - \beta\left(\mathbf{sa} - \mathbf{as} - \frac{2}{3}\{\mathbf{as}\}\mathbf{I}\right) + \gamma(\mathbf{a\omega} - \omega\mathbf{a}), \tag{1}$$

where $\mathbf{a} \equiv a_{ij} \equiv \frac{\overline{u_i'u_j'}}{k} - \frac{2}{3}\delta_{ij}$ is the normalized anisotropic Reynolds-stress tensor, with k as the turbulent kinetic energy, $\overline{u_i'u_j'}$ as the Reynolds-stress tensor and $\mathbf{I} \equiv \delta_{ij}$ as the Kronecker delta. The tensors $\mathbf{s} \equiv s_{ij} \equiv \frac{1}{2}\frac{k}{\varepsilon}(U_{i,j} + U_{i,j})$ and $\omega \equiv \omega_{ij} \equiv \frac{1}{2}\frac{k}{\varepsilon}(U_{i,j} - U_{i,j})$ are the normalized strain-rate tensor and the normalized vorticity tensor, respectively, with $U_{i,j}$ as the mean velocity gradient and ε as the dissipation. In addition, three parameters are present in Eq. 1: α, β and γ, which are a function of the ratio of turbulent production and dissipation: $\mathscr{P}/\varepsilon$, and two constants: C_1 and C_2 that originate from the pressure-strain model of Launder et al. The implicit algebraic equations of Eq. 1 often behave numerically stiffly. Therefore, Pope [10] proposed a method to derive an exact explicit solution which has been adopted by Gatski and Speziale [11] to obtain the full explicit solution in three dimensional space. However, this solution has singularities and is not useful for practical applications. Taulbee [6] made the assumption that $\beta = 0$ to obtain a simplified ARSM and used the method of Pope to derive the corresponding NLEVM. (Note that in the literature these explicit solutions are also referred to as explicit algebraic Reynolds-stress models, however, the term NLEVM will be used in this research.) Apsley and Leschziner [5] used a different approach to obtain an explicit solution. Instead of using the method of Pope, a formal iteration procedure is employed to approximate the full explicit solution.

In the notation of Pope, the explicit solution of Eq. 1 can be written as:

$$\mathbf{a} = \sum_{\lambda=1}^{10} G^{(\lambda)}(\eta_i)\,\mathbf{T}^{(\lambda)}(\mathbf{s},\omega), \tag{2}$$

with ten linearly independent tensors $T^{(\lambda)}$:

$$\begin{array}{lcllcl}
\mathbf{T}^{(1)} &=& \mathbf{s}, & \mathbf{T}^{(6)} &=& \omega^2\mathbf{s} + \mathbf{s}\omega^2 - \frac{2}{3}\{\mathbf{s}\omega^2\}\mathbf{I}, \\
\mathbf{T}^{(2)} &=& \mathbf{s}\omega - \omega\mathbf{s}, & \mathbf{T}^{(7)} &=& \omega\mathbf{s}\omega^2 - \omega^2\mathbf{s}\omega, \\
\mathbf{T}^{(3)} &=& \mathbf{s}^2 - \frac{1}{3}\{\mathbf{s}^2\}\mathbf{I}, & \mathbf{T}^{(8)} &=& \mathbf{s}\omega\mathbf{s}^2 - \mathbf{s}^2\omega\mathbf{s}, \\
\mathbf{T}^{(4)} &=& \omega^2 - \frac{1}{3}\{\omega^2\}\mathbf{I}, & \mathbf{T}^{(9)} &=& \omega^2\mathbf{s}^2 + \mathbf{s}^2\omega^2 - \frac{2}{3}\{\omega^2\mathbf{s}^2\}\mathbf{I}, \\
\mathbf{T}^{(5)} &=& \omega\mathbf{s}^2 - \mathbf{s}^2\omega, & \mathbf{T}^{(10)} &=& \omega\mathbf{s}^2\omega^2 - \omega^2\mathbf{s}^2\omega,
\end{array} \tag{3}$$

$G^{(\lambda)}(\eta_i)$ are scalar functions of invariants η_i. There is a finite number of linearly independent tensor groups because any other higher order tensor, e.q. $\omega\mathbf{s}^3\omega^2 - \omega^2\mathbf{s}^3\omega$, can be written as a linear combination of $T^{(\lambda)}$ employing the Cayley-Hamilton theorem [10]. Any rewritten higher order tensor group will break up into lower order tensors multiplied by invariants which are stored in the scalar functions $G^{(\lambda)}$. In total five linearly independent invariants exist:

$$\eta_1 = \{\mathbf{s}^2\},\ \eta_2 = \{\omega^2\},\ \eta_3 = \{\mathbf{s}^3\},\ \eta_4 = \{\mathbf{s}\omega^2\},\ \eta_5 = \{\mathbf{s}^2\omega^2\}. \tag{4}$$

Due to the linear independence, all tensor groups $T^{(\lambda)}$ must share the properties of $\mathbf{a}$, hence, each $T^{(\lambda)}$ is a second order symmetric deviatoric tensor.

The nonlinear stress-strain relationships in the NLEVM of Taulbee and the NLEVM of Apsley and Leschziner can be written in the form of Eq. 2. The corresponding scalar functions are given in Table 1.

$G^{(\lambda)}$	linear EVM	cubic NLEVM	quartic NLEVM
$G^{(1)}$	$-\alpha$	$-\alpha\left(1+\frac{2}{3}\beta^2\eta_1+2\gamma^2\eta_2\right)$	$-\alpha\left(1-\frac{1}{2}\eta_2\gamma^2\right)/Q$
$G^{(2)}$	0	$\alpha\gamma$	$\alpha\gamma\left(1-2\eta_2\gamma^2\right)/Q$
$G^{(3)}$	0	$2\alpha\beta$	0
$G^{(4)}$	0	0	$-6\alpha\gamma^4\eta_4/Q$
$G^{(5)}$	0	$-3\alpha\beta\gamma$	0
$G^{(6)}$	0	$-3\alpha\gamma^2$	$-3\alpha\gamma^2/Q$
$G^{(7)}$	0	0	$3\alpha\gamma^3/Q$

Table 1: Scalar functions of stress-strain relation of linear EVM and NLEVMs. $G^{(8-10)} = 0$. $Q \equiv \left(1-2\eta_2\gamma^2\right)\left(1-\frac{1}{2}\eta_2\gamma^2\right)$.

2.2 Calibration

The NLEVMs given in Sec. 2.1 include two or three parameters, namely α, β and γ. In theory, the parental ARSM of Eq. 1 defines the parameters. However, the logarithmic region of a boundary layer is not properly described when the same parameters in the NLEVMs are used because the NLEVMs are approximated explicit solutions of the ARSM. Therefore, α, β and γ are determined from calibration. Apsley and Leschziner determined α, β and γ by a calibration with a simple shear flow in which the only non zero components of the strain-rate tensor and the vorticity tensor are: $s_{13} = s_{31} = \frac{1}{2}\tilde{\sigma}$ and $\omega_{13} = -\omega_{31} = \frac{1}{2}\tilde{\sigma}$, respectively. Note that the shear parameter is defined as $\sigma \equiv \frac{k}{\varepsilon}\sqrt{(U_{i,j})^2}$ and the $\sim$ symbol denotes calibration parameters. In addition, the standard atmospheric Cartesian system is used in which the flow direction is x- or 1-axis and the wall normal direction is z- or 3-axis. The normalized anisotropic Reynolds-stress in simple shear flow is defined as:

$$a_{ij} = \begin{bmatrix} \tilde{a}_{11} & 0 & \tilde{a}_{13} \\ 0 & -\tilde{a}_{11}-\tilde{a}_{33} & 0 \\ \tilde{a}_{13} & 0 & \tilde{a}_{33} \end{bmatrix}. \tag{5}$$

Substituting s_{ij}, ω_{ij} and a_{ij}, belonging to the simple shear flow, into Eq. 2 leads to three linearly independent equations for the cubic NLEVM. The solution is derived by Apsley and Leschziner [5] and it is given in Table 2. The same procedure is carried out for the quartic NLEVM of Taulbee. The resulting two linearly independent equations are:

$$\tilde{a}_{11} = \frac{(\alpha\tilde{\sigma})(\gamma\tilde{\sigma})}{\tilde{Q}}\left(1+\frac{1}{4}(\gamma\tilde{\sigma})^2\right), \qquad \tilde{a}_{13} = -\frac{(\alpha\tilde{\sigma})}{\tilde{Q}}\left(1+\frac{1}{4}(\gamma\tilde{\sigma})^2\right), \tag{6}$$

with

$$\tilde{Q} \equiv \left(1+(\gamma\tilde{\sigma})^2\right)\left(1+\frac{1}{4}(\gamma\tilde{\sigma})^2\right), \tag{7}$$

and the solution is also given in Table 2.

	cubic NLEVM	quartic NLEVM
$\alpha\tilde{\sigma}$	$-\tilde{a}_{13}+\sqrt{\tilde{a}_{13}^2+(\tilde{a}_{11}-\tilde{a}_{33})^2-3(\tilde{a}_{11}+\tilde{a}_{33})^2}$	$-2\tilde{a}_{13}\left(1+\left(\frac{\tilde{a}_{11}}{\tilde{a}_{13}}\right)^2\right)$
$\beta\tilde{\sigma}$	$\frac{3(\tilde{a}_{11}+\tilde{a}_{33})}{\alpha\tilde{\sigma}}$	0
$\gamma\tilde{\sigma}$	$\frac{(\tilde{a}_{11}-\tilde{a}_{33})}{\alpha\tilde{\sigma}}$	$-\frac{\tilde{a}_{11}}{\tilde{a}_{13}}$

Table 2: Definition of NLEVM parameters α,β and γ determined by calibration.

2.3 Choice of calibration parameters $\tilde{a}_{11},\tilde{a}_{33},\tilde{a}_{13}$ and $\tilde{\sigma}$

In the previous section the two NLEVMs are calibrated with a simple shear flow. The simple shear flow is characterized by the anisotropic Reynolds-stress components $\tilde{a}_{11},\tilde{a}_{33},\tilde{a}_{13}$ and the shear parameter $\tilde{\sigma}$. The choice of these four constants will determine the scalar functions $G^{(\lambda)}$ in Eq. 2, hence, the model performance of the NLEVM is directly related to $\tilde{a}_{11},\tilde{a}_{33},\tilde{a}_{13}$ and $\tilde{\sigma}$.

For atmospheric flows describing a simple shear flow with $\widetilde{\mathscr{P}/\varepsilon}=1$, it is desired to be able to set the turbulence intensity I_{ref} at the inlet boundary for a certain reference height $z=z_{ref}$. Using the linear $(k-\varepsilon)$ EVM, the turbulence intensity is determined by setting $\tilde{C}_\mu$. Since the solution of the linear $k-\varepsilon$ EVM for the logarithmic region of a simple shear flow for a rough wall is [12]:

$$\frac{U}{u^*}=\frac{1}{\kappa}\ln\left(\frac{z}{z_0}\right),\ k=\frac{u^{*2}}{\sqrt{\tilde{C}_\mu}},\ \varepsilon=\frac{u^{*3}}{\kappa z}, \tag{8}$$

using $U=U_{ref}$ and $z=z_{ref}$, then:

$$I_{ref} \equiv \frac{\sqrt{\frac{2}{3}k}}{U_{ref}}=\tilde{C}_\mu^{-\frac{1}{4}}\sqrt{\frac{2}{3}}\frac{\kappa}{\ln\left(\frac{z_{ref}}{z_0}\right)}. \tag{9}$$

Note that U is the stream-wise mean velocity, u^* is the friction velocity, κ is the Von Karman constant, z is the distance from the wall and z_0 is the wall roughness. In addition, $\tilde{C}_\mu$ is used to distinguish from the (non constant) C_μ present in the NLEVMs. The value of $\tilde{\sigma}$ and $\tilde{a}_{13}$ can be related to $\tilde{C}_\mu$ by using Eq. 8:

$$\tilde{\sigma}=\frac{k}{\varepsilon}\left\|\frac{\partial U}{\partial z}\right\|=\frac{u^*}{\kappa z}=\frac{1}{\sqrt{\tilde{C}_\mu}}, \tag{10}$$

and

$$\left.\begin{aligned}\widetilde{\mathscr{P}/\varepsilon} &\equiv -\{\tilde{\mathbf{a}}\tilde{\mathbf{s}}\}=1\\ &=-2\tilde{a}_{13}\tilde{s}_{13}=-\tilde{a}_{13}\tilde{\sigma}=-\tilde{a}_{13}\tfrac{1}{\sqrt{\tilde{C}_\mu}}\end{aligned}\right\}\Rightarrow \tilde{a}_{13}=-\sqrt{\tilde{C}_\mu}. \tag{11}$$

The other two calibration parameters $\tilde{a}_{11},\tilde{a}_{33}$ cannot be related to $\tilde{C}_\mu$. Instead, either measurements or computation can determine the values of $\tilde{a}_{11},\tilde{a}_{33}$ in simple shear flow with a rough wall. Apsley and Leschziner used a direct numerical simulation of channel flow to obtain wall functions for all four calibration parameters. In this research the asymptotic value (normal wall distance

$\rightarrow \infty$) of $\tilde{a}_{11}, \tilde{a}_{33}$ of the same direct numerical simulation is used [5]: $\tilde{a}_{11} = 0.333$, $\tilde{a}_{33} = -0.263$. In the work of Crespo et al. [7] the NLEVM of Taulbee was calibrated with atmospheric measurements in which $\tilde{a}_{11} = -\tilde{a}_{33} = 0.38$. However, in the current work it is preferred to use the direct numerical simulation data. A consequence of using the calculated calibration parameters with $\tilde{a}_{11} \neq -\tilde{a}_{33}$ for the quartic NLEVM is that the resulting a_{11} and a_{33} for a simple shear flow are not equal to the intended value of the calibration parameters. Instead $a_{11} = \frac{1}{2}(\tilde{a}_{11} - \tilde{a}_{22}) = 0.298$ and $a_{33} = -\frac{1}{2}(\tilde{a}_{11} - \tilde{a}_{22}) = -0.298$.

2.4 Boundedness

The scalar function $G^{(1)}$ of the cubic NLEVM is not bounded. Apsley and Leschziner proposed to use a limiter function $f_P(\sigma)$ for all scalar functions which has been adopted in the present research. Except for $G^{(4)}$, all scalar functions $G^{(\lambda)}$ of the quartic NLEVM are all bounded by the invariant η_2 in the denominator:

$$\begin{aligned} \lim_{\eta_2 \to 0}, G^{(1)} &= -\alpha, \ \lim_{\eta_2 \to 0}, G^{(2)} = \alpha\gamma, \ \lim_{\eta_2 \to 0}, G^{(6)} = -3\alpha\gamma^2 \ \lim_{\eta_2 \to 0}, G^{(7)} = 3\alpha\gamma^3, \quad (12) \\ \lim_{\eta_2 \to -\infty} G^{(1,2,6,7)} &= 0. \end{aligned}$$

The boundedness of the scalar function $G^{(4)}$ is not obvious since it has the invariant η_4 in the numerator, which could hypothetically grow faster than its denominator. $\eta_4 = \{\mathbf{s}\omega^2\}$ is a function of all nine velocity derivatives $U_{i,j}$, however, $\eta_2 = \{\omega^2\}$ is only a function of the off-diagonal velocity derivatives. As a result, the derivatives $U_{\alpha,\alpha}$, present in the nominator of $G^{(4)}$, are not bounded by the denominator. In the flow around a wind turbine, the derivative $\partial U/\partial x$ is large in vicinity of the rotor which might cause unstable behavior of the NLEVM because of $G^{(4)}$. In the test case of Sec. 3 a bounding function for η_4 is found to be redundant. In addition, the limiter function $f_P(\sigma)$ that is used for the cubic NLEVM is not applied to the quartic NLEVM.

2.5 Effective C_μ

The NLEVMs of Sec. 2.1 include a flow-dependent C_μ that is used to define the eddy viscosity: $\mu_T = \rho C_\mu \frac{k^2}{\varepsilon}$. In the notation of Pope the NLEVM can be written as:

$$\mathbf{a} = -2C_\mu \mathbf{s} + \sum_{\lambda=2}^{10} G^{(\lambda)}(\eta_i)\, \mathbf{T}^{(\lambda)}(\mathbf{s}, \omega), \quad (13)$$

where $-2C_\mu\mathbf{s}$ is the linear part of the NLEVMs with an effective C_μ:

$$C_\mu = -\frac{1}{2}G^{(1)} = \begin{cases} \frac{1}{2}\alpha\left(1 + \frac{2}{3}\beta^2\{\mathbf{s}^2\} + 2\gamma^2\{\omega^2\}\right) & \text{(cubic)} \\ \frac{\frac{1}{2}\alpha\left(1 - \frac{1}{2}\{\omega^2\}\gamma^2\right)}{(1 - 2\{\omega^2\}\gamma^2)(2 - \{\omega^2\}\gamma^2)} & \text{(quartic)} \end{cases} \quad (14)$$

The calibration parameters α, β and γ and the first invariant $\{\mathbf{s}^2\}$ are always positive, however, the second invariant is always negative: $\{\omega^2\}$. This means that effective C_μ in the cubic NLEVM is not unconditionally positive. The effective C_μ in the quartic NLEVM is always positive but can still become zero. Apsley and Leschziner made the same observation about their cubic NLEVM and proposed to use a different C_μ in the eddy viscosity relation: $C_\mu = \tilde{C}_\mu f_P$ where f_P is the limiter function used to keep the scalar functions bounded. However, omitting the complete flow-dependent C_μ reduces the model performance. In present research the definition of Eq. 14 is used for both NLEVMs and an unconditional positive and nonzero C_μ is forced by a maximum limiter:

$$C_\mu = \max\left(-\frac{1}{2}G^{(1)}, a\tilde{C}_\mu\right), \quad (15)$$

where a is a positive small number such that $C_\mu \neq 0$, i.e. 1×10^{-4}.

2.6 Implementation

The NLEVMs are implemented as an extension of the linear $k-\varepsilon$ EVM. The nonlinear part of the stress-strain relationship of the NLEVMs is implemented as a momentum source term. The effective C_μ is used to define the eddy viscosity and the transport equations for k and ε used in the linear EVM are also employed for the NLEVMs.

3 WIERINGERMEER TEST CASE

The cubic and quartic NLEVMs are used to simulate the wake of a single wind turbine. Wake measurements from the Wind Turbine Test Site Wieringermeer (EWTW), owned by the Energy Research Centre of the Netherlands (ECN), are used to compare with the numerical simulations. The results of almost 5 years of measurements have been published by Schepers [13]. In addition, the 10 minute averaged data was made available for this research. In the two subsequent sections, a brief overview of the site is presented and the choice of input parameters for the numerical simulations are motivated. The single wake simulations are discussed in Sec. 3.3.

3.1 Site overview

EWTW is located in the North West of the Netherlands. The landscape mainly consist of flat farmland. 2 km East from the meteorological mast a large lake (IJsselmeer) is present. The land and the lake are separated by a dike which is 8 m and 3 m tall with respect to the land and the lake, respectively.

The meteorological mast is located South of five 2.5 MW wind turbines with a 80 m rotor diameter and hub height. The layout of the five wind turbines is given in Fig. 1. Two single wake cases are measured for wind directions around 31°and 315°with a corresponding downstream distance of 2.5D and 3.5D, respectively.

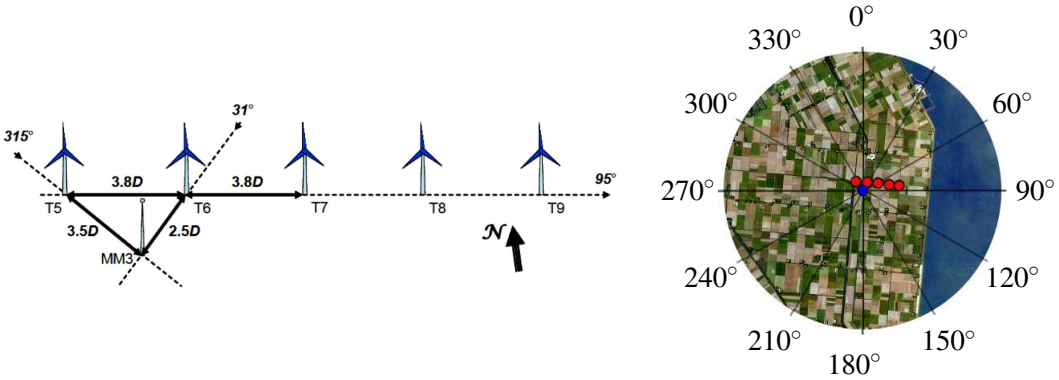

Figure 1: Research wind turbines at EWTW site. Left: geometrical sketch, source: [13]. Right: satellite image of 4 km radius around meteorological mast MM3 (blue dot), five red dots: research wind turbines, source: Google Earth.

3.2 Input parameters for numerical simulations

In order to compare the measurements with the numerical simulations the following input parameters for the numerical simulations are necessary: the undisturbed stream-wise wind speed at hub height $U_{H,\infty}$, the undisturbed friction velocity u^*, the thrust coefficient C_T, the undisturbed turbulence intensity at hub height $I_{H,\infty}$ and the roughness height z_0. The estimated input parameters are listed in Table 3 and are motivated in subsequent sections.

wake case	2.5D													3.5D
$U_{H,\infty}$ [m/s]	10.9													10.7
C_T [-]	0.63													0.63
dir. [°]	1	6	11	16	21	26	31	36	41	46	51	56	61	285-345
z_0 [cm]	13	11	9.1	7.0	5.5	4.3	3.4	2.8	2.4	2.1	1.9	1.2	0.94	3.0
u^* [m/s]	0.68	0.66	0.64	0.62	0.60	0.58	0.56	0.55	0.54	0.53	0.52	0.50	0.48	0.54
$I_{H,\infty}$ [%]	7.8	7.5	7.3	7.1	7.0	6.9	6.8	6.7	6.7	6.6	6.6	6.5	6.4	10

Table 3: Summary of input parameters for numerical computations of the two single wake cases.

Undisturbed velocity
The meteorological mast is instrumented with sonic anemometers, cups and vanes at 80 m. Unfortunately, upstream measurements are not carried out. Therefore, the upstream undisturbed wind speed at hub height is estimated from power measurements of wind turbine T5 (3.5D case) and wind turbine T6 (2.5D case). Only data with undisturbed wind speeds between 10-12 m/s are selected. The average of the wind speed between 1-61°and 285-345°, corresponding to the two single wake cases, are 10.9 m/s and 10.7 m/s, respectively.

Friction velocity
The friction velocity is calculated with the log law: $u^* = U_{H,\infty}\kappa/\ln(z_H/z_0)$.

Atmospheric stability
The lack of upstream measurements makes it impossible to identify and disregard non-neutral atmospheric measurements. However, the probability of a near neutral atmospheric boundary layer increases with high wind speeds, i.e. 10-12 m/s.

Thrust coefficient
The thrust coefficient curve is measured and calculated by Schepers [14]. The measurements are based on the tower bending moment and the calculations are carried out with PHATAS [15]. Both methods estimate at thrust coefficient of 0.63 for the averaged undisturbed wind speeds of 10.7 m/s and 10.9 m/s.

Turbulence intensity
Since there is a the lack of upstream measurements an estimation of the undisturbed inflow turbulence intensity for the 3.5D case is made by averaging the corresponding closest 'undisturbed' sector. Between 250°and 280°the average turbulence intensity is equal to 10%. Note that only undisturbed wind speeds between 10-12 m/s are considered. The turbulence intensities for North Eastern winds are calculated by a number of precursor simulations, as discussed in the following section.

Roughness height
For Western winds the roughness is dictated by flat farmland with sparse larger vegetation, as shown in Fig. 1. By physical inspection the roughness height is estimated to be 0.03 m. For Eastern winds the roughness height is affected by the lake and the farmland. Therefore, the streamwise velocity profile at the location of wind turbine T6 is calculated with a RANS precursor simulation of the most important terrain features: the water to land roughness change, the height difference between the land and the water and a Gaussian shaped dike. EllipSys3D is used as flow solver [16]. In total thirteen different wind directions are investigated between 1-61°with equidistant intervals. At the inflow a loglaw profile is prescribed where the friction velocity is set such that the hub height velocity at the original wind turbine location is approximately equal

to the measured average of 10.9 m/s (deviations are within 0.3%). The linear $k-\varepsilon$ turbulence model is used with constants that are applicable for atmospheric terrain flows, i.e. $C_\mu = 0.03$ and $C_{\varepsilon 1} = 1.21$ [16].

All precursor simulations show that the wind turbine rotor is operating in the transition zone between the inner boundary layer, caused by the roughness change and the outer boundary layer. The velocity profile in the mixing layer is approximated by a logarithmic profile based on linear curve fit between 60 m and 100 m in the $ln(z)-u$ domain. From the curve fit the effective friction velocity and the effective roughness height are calculated. The results for all thirteen wind direction are listed in Table 3 and will be used in the wake simulations. Note that the non-equilibrium profile could also be used directly as an input for the wake simulations, however, the NLEVMs show numerically unstable behavior when the non-equilibrium profile is prescribed at the inlet. Therefore, only the fitted logarithmic profile belonging to the mixing layer will be used as inlet condition.

3.3 Numerical simulations

The two measured wake cases (2.5D and 3.5D) are simulated with RANS using three different turbulence models: the linear $k-\varepsilon$ EVM and the two NLEVMs from Sec. 2.

Method

The in-house incompressible finite volume code EllipSys3D is used as flow solver [16].

The wind turbine is modeled as an Actuator Disk (AD) [17] on which the blade forces are distributed in the radial direction and constant in the circumferential direction. The real blade forces of the research wind turbines of EWTW are not available. Therefore, the force distribution of the NREL 5 MW reference wind turbine blade, calculated with a detached eddy simulation, is used in which the total thrust force is scaled with C_T.

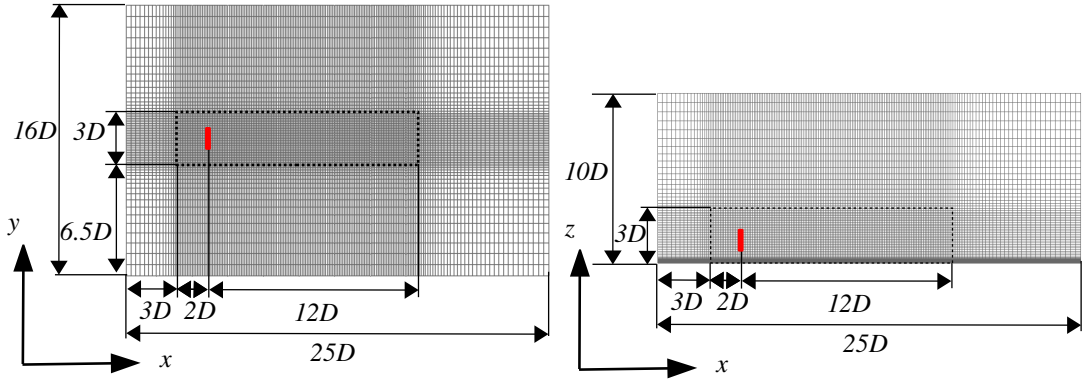

Figure 2: Computational domain. Left: top view. Right: side view. Dotted black box marks the wake domain. Actuator disk is illustrated as a red filled box. One in every two nodes is shown.

The AD is placed in a box shaped domain of dimensions: 25D $\times$ 16D $\times$ 10D, as shown in Fig. 2. In total $192 \times 64 \times 96 = 1.18$ million cells are used to discretize the domain. The wall at $z = 0$ is modeled as a rough wall where the first cell height is in the order of the roughness height. The boundaries at $x = 0$ and $x = 25$D is an inlet and an outlet, respectively. At the inlet a stream-wise logarithmic profile is specified. The top boundary at $z = 10$D and the side boundaries at $y = 0$ and $y = 16$D are modeled as symmetric walls. Around the AD a wake domain of dimensions: 14D $\times$ 3D $\times$ 3D is defined where uniform spacing of ten cells per diameter is applied in all directions. (Below $z = \frac{1}{2}z_H$ the cells in the wall normal direction are refined due to the presence of the wall.) A mesh study has shown that ten cells per diameter is sufficient [17]. Outside the wake domain stretching is allowed with a maximum edge growth ratio of 1.2.

The input parameters from Table 3 are used in the AD simulations. However, the NLEVMs show numerically unstable behavior for a turbulence intensity of 10%. (Note that the instabilities are also seen when the AD is switched off and they are not related to the unboundedness of $G^{(4)}$ of the quartic NLEVM.) Therefore, the 3.5D wake case is simulated with a turbulence intensity of 8% such that a comparison between the turbulence models can be made. The 2.5D wake case is performed with thirteen simulations corresponding to wind directions between 1-61°with uniform intervals. One AD simulation is conducted for the 3.5D wake case.

The turbulence intensity is set through C_μ by using Eq. 9 and the logarithmic solution is preserved by adapting $C_{\varepsilon,1}$ as: $C_{\varepsilon,1} = C_{\varepsilon,2} - \kappa^2/\left(\sqrt{C_\mu}\sigma_\varepsilon\right)$. The other turbulence constants in the transport equations for k and ε are chosen to be: $C_{\varepsilon,2} = 1.92$, $\kappa = 0.40$, $\sigma_\varepsilon = 1.30$ and $\sigma_k = 1.00$.

Standard values for the density and the dynamic fluid viscosity are used: $\rho = 1.225$ kg/m^3 and $\mu = 1.784 \times 10^{-5}$ kg/(m.s).

Results

The results of the numerical simulations are plotted with the results of the measurements in Fig. 3. For each wake case, three quantities at hub height are plotted against the relative wind direction, namely: the stream-wise velocity $U/U_{H,\infty}$, the stream-wise Reynolds-stress $\sqrt{\overline{u'u'}}/U_{H,\infty}$ and the vertical Reynolds-stress $\sqrt{\overline{w'w'}}/U_{H,\infty}$.

2.5D case

For the 2.5D case the linear EVM under predicts the measured wake deficit by 20% as shown in Fig. 3a. The NLEVMs calculate a much deeper wake deficit compared to the linear EVM but still under predicted the measured one by 5-10%. The reason for the improved performance is further explained in the paragraph: *Influence of effective* C_μ.

The wake at 2.5D is slightly asymmetric. Schepers [13] hypothesized that as this site the asymmetry of wake is caused by terrain effects. The hypothesis is confirmed by all three turbulence models in which a similar wake asymmetry is seen. Thus, the directional dependency of the wind profile and the turbulence intensities, calculated by the precursor field simulations, are capturing the dominant terrain effects.

The Reynolds-stresses calculated by the NLEVMs are closer to the measured Reynolds-stresses compared the ones calculated by the linear EVM. The vertical Reynolds-stress $\sqrt{\overline{w'w'}}/U_{H,\infty}$ from Fig. 3e calculated by the linear EVM is roughly 25% higher than the measured ones, also outside the wake. The main reason for the offset is coming from the fact that the linear EVM is isotropic ($a_{\alpha\alpha} = 0$ in simple shear) and can only be tuned for the undisturbed turbulent kinetic energy. The NLEVMs match the measurements better because the NLEVMs include normal Reynolds-stresses anisotropy. The stream-wise Reynolds-stress $\sqrt{\overline{u'u'}}/U_{H,\infty}$ from Fig. 3c calculated by the NLEVM simulations still unpredicted the magnitude of the measured Reynold-stresses.

3.5D case

As mentioned before, the NLEVMs show numerically unstable behavior in the 3.5D wake case when the measured turbulence intensity of 10% is used. Therefore, the numerical simulations cannot directly be compared with the measurements. Compared to the wake deficit of the 2.5D case, the results of the linear EVM are even more different from the results of the NLEVMs, as seen in Fig. 3b. The wake deficit calculated by the NLEVMs is 15% larger then the one calculated by the linear EVM. Similar observations can be made about the Reynolds-stress as done for the 2.5D case. The asymmetry of the measured wake deficit are not induced by terrain effects [13]. Zahle and Sørensen concluded that the combination of shear and wake rotation can cause wake asymmetry [18]. However, a similar effect is not seen in the current simulations even though rotational forces are applied on the AD.

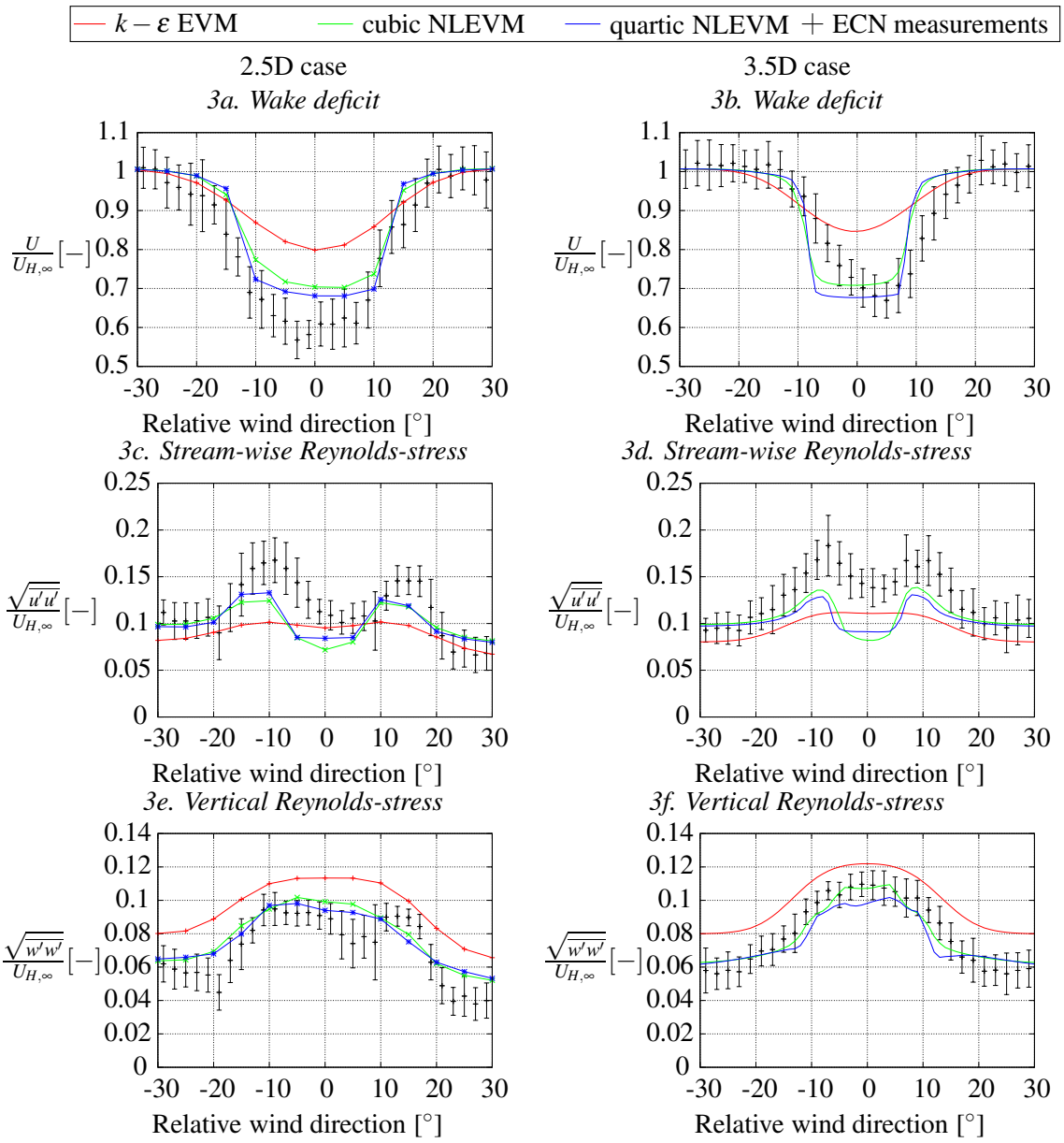

Figure 3: Wake deficit and Reynolds-stresses at hub height for relative wind directions. Left: 2.5D case with $U_{H,\infty} = 10.9$ m/s, right: 3.5D case with $U_{H,\infty} = 10.7$ m/s. The measurements include error bars of one standard deviation. For 3.5D case: measured: $I_{H,\infty} = 10\%$ and the simulation are carried out with $I_{H,\infty} = 8\%$.

Influence of effective C_μ

The wake deficit calculated by the NLEVMs is much larger compared to the linear EVM. The main reason for the difference is the effective, flow-dependent C_μ of Eq. 14. Within 1D downstream of the at $z = z_H + 0.5D$, a large positive peak of normalized mean velocity gradient $k/\varepsilon \partial u/\partial z$ is present. This gradient is the dominant term in the two invariants $\eta_1 \approx -\eta_2 \approx 1/2\,(k/\varepsilon \partial u/\partial z)^2$. Without the limiter function of Eq. 15, the effective C_μ in the cubic model for the 2.5D wake case at 31°becomes negative:

$$C_\mu \approx \frac{1}{2}\alpha\left(1 + \left(\frac{k}{\varepsilon}\frac{\partial u}{\partial z}\right)^2\left(\frac{1}{3}\beta^2 - \gamma^2\right)\right) \approx -6. \tag{16}$$

Hence, the limiter function is active and the effective C_μ is equal to $1 \times 10^{-4}\tilde{C}_\mu$. As a result, the turbulent eddy viscosity $\mu_T = \rho C_\mu \frac{k^2}{\varepsilon}$ in the cubic NLEVM, is decreased downstream of the AD and the NLEVM behaves less dissipative compared to the linear EVM. A similar conclusion can be made about the quartic NLEVM in which the lowest effective C_μ is equal to $\approx 1 \times 10^{-3}$.

Using the proposed C_μ formulation of Apsley and Leschziner, in which C_μ is flow-dependent: $C_\mu = \tilde{C}_\mu f_P(\sigma)$ through the limiter function $f_P(\sigma)$, the eddy viscosity is also lowered downstream of the AD, since the shear parameter is large: $\sigma^2 \approx (k/\varepsilon \partial u/\partial z)^2$. However, the decrease of eddy viscosity is less compared to using the true effective C_μ of Eq. 14.

Wake recovery

In Fig. 4 the stream-wise velocity $U/U_{H,\infty}$ at hub height at a relative wind direction of 0°is plotted against the stream-wise downstream distance $(x-x_{AD})/D$ for all three turbulence models and both wake cases. Except for undisturbed turbulence intensity at hub height, the simulation parameters used in the two wake cases are similar, as listed in Table 3 (31°and 285-245°). Hence, the influence of $I_{H,\infty}$ on performance of the turbulence models can be investigated. The wake recovery calculated by the linear $k-\varepsilon$ EVM is faster with increasing turbulence intensity, however, the opposite is observed for the NLEVMs. Higher turbulence levels should enhance mixing which accelerates the wake recovery. Therefore, the NLEVMs show unphysical behavior towards changes of $I_{H,\infty}$. The unphysical behavior is caused by the flow-dependent C_μ. For higher undisturbed turbulence intensities, the largest derivative $k/\varepsilon \partial u/\partial z$ increases, which lowers the flow-dependent C_μ, as discussed in the previous paragraph. As a result, the eddy viscosity decreases with increasing undisturbed turbulence intensity and the wake recovery is delayed.

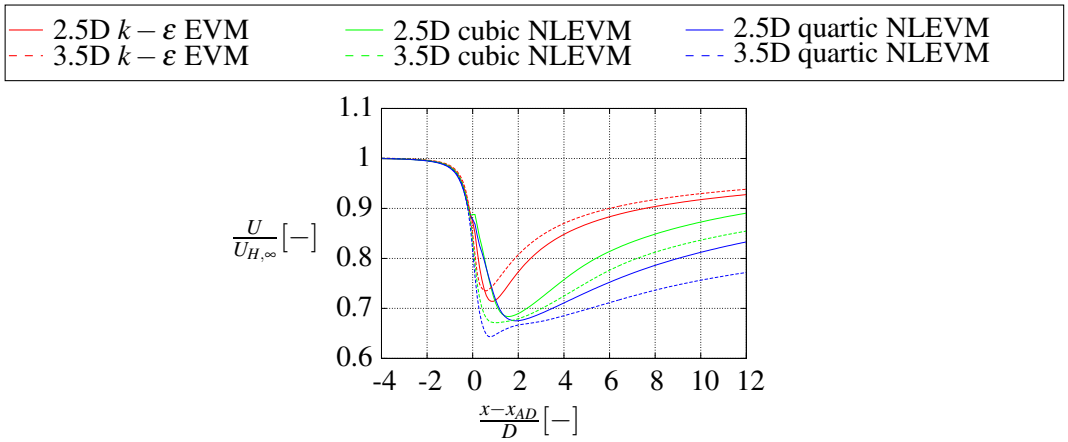

Figure 4: Wake deficit recovery at hub height at a relative wind direction of 0°. 2.5D case: $I_{H,\infty} = 6.8\%$ and 3.5D case: $I_{H,\infty} = 8\%$.

4 CONCLUSION

The linear $k-\varepsilon$ EVM and modified versions of the cubic NLEVM of Apsley and Leschziner and the quartic NLEVM of Taulbee are tested and compared with wake measurements from Wieringermeer for two single wake cases: 2.5D and 3.5D at different wind directions. In the 2.5D case the performance of the NLEVMs is much better compared to the linear EVM, however, the wake deficit and the stream-wise Reynolds-stress are still under predicted compared to the measurements. The numerically unstable behavior of the NLEVMs at high turbulence intensities makes it impossible to simulate the 3.5D case with the observed-based undisturbed turbulence intensity of 10%. Not having the full flexibility of setting the undisturbed turbulence intensity is a major drawback of the NLEVMs. The 3.5D case is simulated by all three turbulence models with a turbulence intensity of 8%. In terms of wake deficit and Reynolds-stresses, the difference between

the linear EVM and the two NLEVMs is even larger compared to the 2.5D case.

The performance increase of the NLEVMs is caused by the flow-dependent C_μ which lowers the eddy viscosity downstream of the AD. Unfortunately, the flow-dependent C_μ is also responsible for predicting a faster wake recovery for lower undisturbed turbulence intensities, which is unphysical behavior.

REFERENCES

[1] R. J. Barthelmie, S. T. Frandsen, N. M. Nielsen, S. C. Pryor, P.-E. Réthoré, and H. E. Jørgensen, "Modelling and measurements of power losses and turbulence intensity in wind turbine wakes at middelgrunden offshore wind farm," *Wind Energy*, vol. 10, pp. 217–228, 2007.

[2] N. Troldborg, G. C. Larsen, H. A. Madsen, K. S. Hansen, J. N. Sørensen, and R. Mikkelsen, "Numerical simulations of wake interaction between two wind turbines at various inflow conditions," *Wind Energy*, vol. 14, p. 859876, 2011.

[3] P.-E. Réthoré, *Wind Turbine Wake in Atmospheric Turbulence*. PhD thesis, Risø, 2009.

[4] M. J. Boussinesq, *Théorie de l'écoulement tourbillonnant et tumultueux des liquides*. Gauthier-Villars et fils, 1897.

[5] D. D. Apsley and M. A. Leschziner, "A new low-reynolds-number nonlinear two-equation turbulence model for complex flows," *International Journal of Heat and Fuid Flow*, vol. 19, pp. 209–222, 1998.

[6] D. B. Taulbee, "An improved algebraic reynolds stress model and corresponding nonlinear stress model," *Physics of Fluids*, vol. A4 11, pp. 2555–2561, 1992.

[7] A. Crespo, R. Gómez-Elvira, E. Migoya, F. Manuel, and H. J., "Anisotropy of turbulence in wind turbine wakes," *Journal of Wind Engineering and Industrial Aerodynamics*, vol. 93, pp. 797–814, 2005.

[8] W. Rodi, "A new algebraic relation for calculating the reynolds stress," *Zeitschrift for angewandte mathematik und mechanik*, vol. 56, pp. 227–238, 1976.

[9] B. E. Launder, G. J. Reece, and W. Rodi, "Progress in the development of a reynolds-stress turbulence closure," *Jounal of Fluid Mechanics*, vol. 68, pp. 537–566, 1975.

[10] S. B. Pope, "A more general effective-viscosity hypothesis," *Jounal of Fluid Mechanics*, vol. 72, pp. 331–440, 1975.

[11] T. B. Gatski and C. G. Speziale, "On explicit algebraic models for complex turbulent flows," *Jounal of Fluid Mechanics*, vol. 254, pp. 59–78, 1993.

[12] P. J. Richards and R. P. Hoxey, "Appropriate boundary conditions for computational wind engineering models using the $k-\varepsilon$ turbulence model," *Journal of Wind Engineering and Industrial Aerodynamics*, vol. 46,47, pp. 145–153, 1993.

[13] J. G. Schepers, "Analysis of wake measurements from the ECN wind turbine test site wieringermeer, EWTW," *Wind Energy*, vol. 15, p. 575591, 2012.

[14] J. G. Schepers, "Personal communication," 2012.

[15] C. Lindenburg and H. Snel, "PHATAS-II: program for horizontal axis wind turbine analysis and simulation version II," tech. rep., ECN-C–93-038, 1993.

[16] N. N. Sørensen, *General purpose flow solver applied to flow over hills*. PhD thesis, Technical University of Denmark, 1994.

[17] P.-E. Réthoré, M. P. van der Laan, N. Troldborg, F. Zahle, and N. N. Sørensen, "Verification and validation of an actuator disc model," *Wind Energy*, 2013.

[18] F. Zahle and N. N. Sørensen, "Overset grid flow simulation on a modern wind turbine," in *AIAA-2008-6727*, 2008.